Since January 2020 Elsevier has created a COVID-19 resource centre with free information in English and Mandarin on the novel coronavirus COVID-19. The COVID-19 resource centre is hosted on Elsevier Connect, the company's public news and information website.

Cell Reports

Article

IFP35 as a promising biomarker and therapeutic target for the syndromes induced by SARS-CoV-2 or influenza virus

Graphical abstract

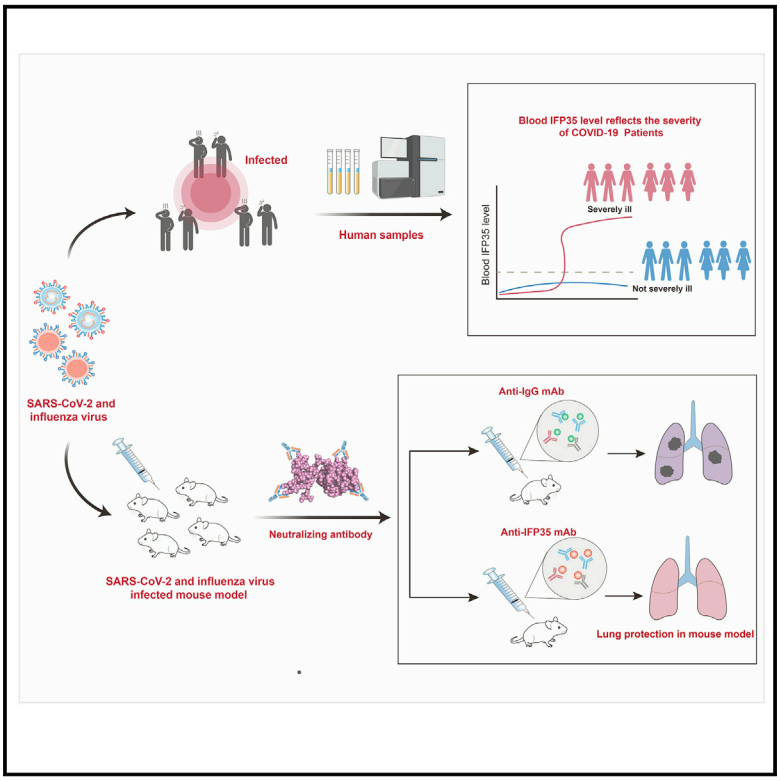

Highlights

- Serum IFP35 levels in individuals with SARS-CoV-2 correlate with severity of the syndrome
- IFP35 is released by macrophages and lung epithelial cells under influenza infection
- IFP35 neutralizing antibodies reduce lung injury and mortality of infected mice
- IFP35 serves as a biomarker and as a therapeutic target in virus-induced syndromes

Authors

Yang Yu, Na Xu, Qi Cheng, ..., Yingfang Liu, Xiaoping Chen, Huanhuan Liang

Correspondence

lanping@mail.sysu.edu.cn (P.L.), zlshi@wh.iov.cn (Z.S.), liuyingf5@mail.sysu.edu.cn (Y.L.), chenxpchenxp@163.com (X.C.), lianghh26@mail.sysu.edu.cn (H.L.)

In brief

Yu et al. identify IFP35 as a biomarker and as a therapeutic target in SARS-CoV-2- or influenza virus-induced syndromes. Neutralizing antibodies against IFP35 considerably reduces lung injury and the mortality of infected mice.

Yu et al., 2021, Cell Reports *37*, 110126
December 21, 2021
https://doi.org/10.1016/j.celrep.2021.110126

CellPress

Cell Reports

CellPress
OPEN ACCESS

Article

IFP35 as a promising biomarker and therapeutic target for the syndromes induced by SARS-CoV-2 or influenza virus

Yang Yu,[1,16] Na Xu,[2,16] Qi Cheng,[3,4,16] Fei Deng,[5,16] Meiqin Liu,[6,7,16] Airu Zhu,[8] Yuan-Qin Min,[5] Dan Zhu,[9] Wenbo Huang,[8] Xu Feng,[2] Xizhong Jing,[1] Ying Chen,[6,7] Daoyuan Yue,[10] Yawei Fan,[3,4] Chang Shu,[3,4] Qing Guan,[10] Zifeng Yang,[8] Jincun Zhao,[8] Wenjun Song,[11] Deyin Guo,[1] Huanliang Liu,[12,13] Jindong Zhao,[14] Ping Lan,[12,*] Zhengli Shi,[6,*] Yingfang Liu,[1,12,17,*] Xiaoping Chen,[3,4,15,*] and Huanhuan Liang[2,*]

[1]School of Medicine, Sun Yat-Sen University, Shenzhen, Guangdong 518107, China
[2]School of Pharmaceutical Science (Shenzhen), Sun Yat-Sen University, Shenzhen, Guangdong 518107, China
[3]Hepatic Surgery Center, Tongji Hospital, Tongji Medical College, Huazhong University of Science and Technology, Wuhan, Hubei 430030, China
[4]Hubei Key Laboratory of Hepato-Pancreato-Biliary Diseases, Wuhan, Hubei 430030, China
[5]State Key Laboratory of Virology and National Virus Resource Center, Wuhan Institute of Virology, Chinese Academy of Science, Wuhan, Hubei 430071, China
[6]CAS Key Laboratory of Special Pathogens, Wuhan Institute of Virology, Center for Biosafety Mega-Science, Chinese Academy of Science, Wuhan 430071, China
[7]University of Chinese Academy of Sciences, Beijing 100049, China
[8]State Key Laboratory of Respiratory Disease, National Clinical Research Center for Respiratory Disease, Guangzhou Institute of Respiratory Health, the First Affiliated Hospital of Guangzhou Medical University, Guangzhou, Guangdong 510120, China
[9]Department of Cardiology and Institute of Vascular Medicine, Peking University Third Hospital, NHFPC Key Laboratory of Cardiovascular Molecular Biology and Regulatory Peptides; Key Laboratory of Molecular Cardiovascular Science, Ministry of Education; Beijing Key Laboratory of Cardiovascular Receptors Research. Beijing 100191, China
[10]Department of Laboratory Medicine, Tongji Hospital, Tongji Medical College, Huazhong University of Science and Technology, Wuhan, Hubei 430030, China
[11]State Key Laboratory of Respiratory Disease, Institute of Integration of Traditional and Western Medicine, Guangzhou Medical University, Guangzhou, Guangdong 510180, China
[12]Department of Colorectal Surgery, The Sixth Affiliated Hospital, Sun Yat-sen University, Guangdong Institute of Gastroenterology, Guangdong Provincial Key Laboratory of Colorectal and Pelvic Floor Diseases, Guangzhou, Guangdong 510655, China
[13]Department of Clinical Laboratory, The Sixth Affiliated Hospital, Sun Yat-sen University, Guangzhou, Guangdong 510655, China
[14]State Key Laboratory of Protein and Plant Genetic Engineering, College of Life Sciences, Peking University, Beijing 100871, China
[15]Key Laboratory of Organ Transplantation, Ministry of Education, NHC Key Laboratory of Organ Transplantation, Key Laboratory of Organ Transplantation, Chinese Academy of Medical Sciences, Wuhan, Hubei 430030, China
[16]These authors contributed equally
[17]Lead contact
*Correspondence: lanping@mail.sysu.edu.cn (P.L.), zlshi@wh.iov.cn (Z.S.), liuyingf5@mail.sysu.edu.cn (Y.L.), chenxpchenxp@163.com (X.C.), lianghh26@mail.sysu.edu.cn (H.L.)
https://doi.org/10.1016/j.celrep.2021.110126

SUMMARY

Previous studies have shown that the high mortality caused by viruses such as severe acute respiratory syndrome coronavirus 2 (SARS-CoV-2) and influenza virus primarily results from complications of a cytokine storm. Therefore, it is critical to identify the key factors participating in the cytokine storm. Here we demonstrate that interferon-induced protein 35 (IFP35) plays an important role in the cytokine storm induced by SARS-CoV-2 and influenza virus infection. We find that the levels of serum IFP35 in individuals with SARS-CoV-2 correlates with severity of the syndrome. Using mouse model and cell assays, we show that IFP35 is released by lung epithelial cells and macrophages after SARS-CoV-2 or influenza virus infection. In addition, we show that administration of neutralizing antibodies against IFP35 considerably reduces lung injury and, thus, the mortality rate of mice exposed to viral infection. Our findings suggest that IFP35 serves as a biomarker and as a therapeutic target in virus-induced syndromes.

INTRODUCTION

Regular outbreaks of infectious diseases caused by respiratory viruses such as influenza virus and coronaviruses pose a significant threat to human health (Belongia and Osterholm, 2020; Gostin and Salmon, 2020). The ability of viruses to mutate frequently results in loss of efficacy of existing antiviral drugs and vaccines (Hou et al., 2020; Petrova and Russell, 2018;

Shinde et al., 2021). As observed in the sera of individuals critically ill with coronavirus disease 2019 (COVID-19) or influenza, pro-inflammatory cytokines, including tumor necrosis factor (TNF) and interleukin-6 (IL-6) are increased significantly compared with levels in uninfected people (Buszko et al., 2020; Song et al., 2020; Zhu et al., 2020). In these infected individuals, onset of cytokine storm represents deterioration of the disease to acute respiratory distress syndrome (ARDS), a life-threatening condition associated with lung injury (Bosmann and Ward, 2013; Florescu and Kalil, 2014; Mulchandani et al., 2021; Tang et al., 2020; Zhou et al., 2020a). Thus, immunomodulators to dampen the cytokine storm will be of benefit when they are used in combination with antiviral drugs.

A number of immunotherapies are currently available to treat virus-induced cytokine storm, including corticosteroids, which systematically suppresses the immune system, and cytokine antibodies, which directly target cytokines, such as IL-6, TNF, and granulocyte-macrophage colony-stimulating factor (GM-CSF) (Arabi et al., 2018; De Luca et al., 2020; Delaney et al., 2016; Gokhale et al., 2021; Luo et al., 2020; Salama et al., 2021; Soin et al., 2021; Stone et al., 2020). Although these therapies have been used in emergencies to alleviate lung injury caused by excessive inflammation, a large-scale clinical trial has shown that administration of these anti-inflammatory drugs alone fails to yield high-level efficacy (https://www.roche.com/media/releases/med-cor-2020-07-29.htm). These results indicate that other inflammatory factors are also involved in virus-induced syndromes.

Increasing evidence suggests that damage-associated molecular patterns (DAMPs) are crucial in inflammatory regulation processes (Gong et al., 2020; Zhang et al., 2010). DAMPs activate nuclear factor κB (NF-κB), mitogen-activated protein kinases, as well as other pathways by interacting with pathogen recognition receptors (PRRs) and subsequently induce production of pro-inflammatory cytokines, which further exacerbate inflammatory responses and cause organ damage (Cicco et al., 2020; Harris and Raucci, 2006; Vourc'h et al., 2018). Previous reports have suggested that respiratory virus infection results in release of large amounts of pro-inflammatory DAMPs (Land, 2021; Patel et al., 2018; Samy and Lim, 2015). We propose that targeting DAMPs is a potentially effective approach for life-saving treatment of influenza and COVID-19.

We reported recently that interferon-induced protein 35 (IFP35) is released by macrophages stimulated by lipopolysaccharide (LPS) or bacteria (Xiahou et al., 2017). The released IFP35 is recognized by Toll-like receptor 4 (TLR-4); as a result, the NF-κB pathway is activated, enhancing the overall inflammatory response. Knockout of *Ifp35* alleviates the inflammatory response and increases the survival rate of mice in a LPS-induced sepsis shock model. Here we set out to examine the functions of IFP35 in severe syndromes induced by severe acute respiratory syndrome coronavirus 2 (SARS-CoV-2) or influenza virus. Our analysis showed that the concentration of serum IFP35 was highly related to the severity of COVID-19. In addition, administration of neutralizing antibodies against IFP35 dramatically attenuated lung injury and the mortality rate in SARS-CoV-2- and influenza virus-infected mice.

RESULTS

Clinical characteristics and classification of the individuals with COVID-19

We collected and systematically analyzed the sera of 150 individuals with COVID-19. To simplify the subsequent analysis, we classified individuals with mild and ordinary disease as not severely ill and individuals with severe and critical disease as severely ill. The individuals were divided into two groups (Figure 1A). Group 1 included 112 individuals whose sera were collected on admission. 83 and 29 patients in group 1 were classified as severely ill and not severely ill, respectively (Table S1). Group 2 included 38 individuals whose sera were collected after 4–34 days of treatment in hospital. The average ages of the individuals in group 1 and group 2 were 64 (31–87 years) and 62 (35–84 years), respectively. The age distribution of the individuals is shown in Figure 1B, with 73% of severely ill individuals and 55% of not severely ill individuals being older than 60 years. In addition, we collected the sera of 40 uninfected donors with similar gender and age distributions as control samples.

Severe incidence in group 1 and group 2 was 74% (83 of 112) and 76% (29 of 38), respectively. After 4–34 days of treatment, the health of 80.3% individuals (90 of 112) in group 1 improved, including all not severely ill (29 of 112) and 61 (61 of 112) severely ill individuals. 13.4% (15 of 112) severely ill individuals were worse, and 6.3% (7 of 112) died. The rates of improvement, worsening, and death in group 2 were 65.8% (25 of 38), 5.3% (2 of 38), and 28.9% (11 of 38), respectively. A statistical analysis was performed for the basic physiological conditions of the individuals in group 1 (Table S5). The blood parameters from 112 individuals with COVID-19 are shown as a heatmap in Figure 1C. Consistent with the results described in previous reports (Guan et al., 2020; Liu et al., 2020), we found lymphocytopenia, elevated C-reactive protein (CRP), lactose dehydrogenase (LDH), procalcitonin (PCT), and D-dimer in severely ill individuals. For instance, the average count of lymphocytes in uninfected donors was 1.1–3.8 × 10^9/L. However, the average count of lymphocytes in the 83 severely ill individuals in group 1 was 1.08 ± 0.60 × 10^9/L. Elevated CRP (≥10 μg/mL), LDH (≥250 U/L), PCT (≥0.05 ng/mL), and D-dimer (≥0.5 μg/mL) in severely ill individuals were 72.3%, 73.5%, 71.1%, and 78.3%, respectively. Detailed information for all individuals and uninfected donors is shown in Tables S1–S4.

Blood IFP35 levels reflect the severity of COVID-19

To study whether IFP35 is involved in the pathogenic process of COVID-19, we tested the concentrations of blood IFP35 in the patients of group 1 using an enzyme-linked immunosorbent assay (ELISA). As shown in Figure 1D, the blood levels of IFP35 in 40 uninfected donors were below 150 pg/mL, the detection limit (average, 46 ± 16 pg/mL). Similar results were also observed in the 29 not severely ill individuals, with only six individuals' blood IFP35 levels higher than 150 pg/mL (average, 171 ± 59 pg/mL). However, we found that the average serum concentrations of IFP35 in 81.9% severely ill individuals (68 of 83) were higher than 150 pg/mL, with the average reaching a high level of 950 ± 135 pg/mL. For comparison, we also measured serum IL-6 levels, recognized previously as a

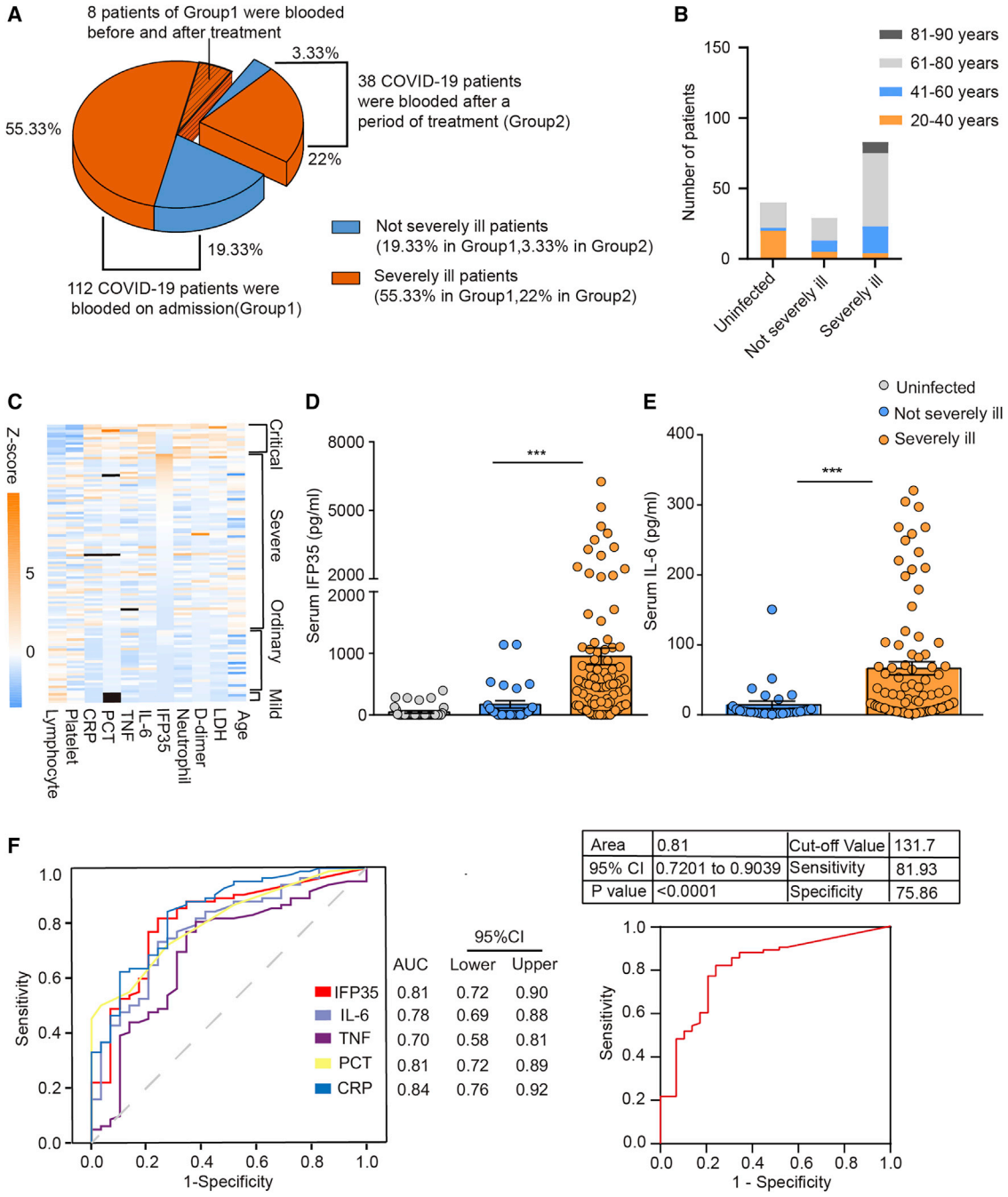

Figure 1. Examination of serum IFP35 in 112 individuals with COVID-19

(A) 150 individuals with COVID-19 were divided into group 1 and group 2 according to their blood draw time.

(B) The age distribution in healthy individuals and those with COVID-19 in group 1.

(C) Heatmap of blood parameters from 112 individuals with COVID-19 and *Z* score ($Z = (x - \mu)/\sigma$) of blood parameters in individuals with critical, severe, ordinary, and mild COVID-19. Each cell represents an individual, and a black cell means the data were not available. The cases of each group are listed in the heatmap in descending order of IFP35 serum concentration.

(D and E) ELISA results of IFP35 (D) and IL-6 (E) in the sera of individuals with COVID-19 in group 1 (uninfected people, n = 40; not severely ill individuals, n = 29; severely ill individuals, n = 83). Significance was calculated by nonparametric Mann-Whitney *U* test. ***p < 0.001, **p < 0.01; ns, no significance.

(F) ROC curve of IFP35, IL-6, TNF, PCT, and CRP comparing severely ill cases (n = 83) and not severely ill cases (n = 29). Area of ROC curve, 95% confidence interval (CI), cutoff value, and sensitivity and specificity of the cut off value are shown in the table.

biomarker indicating the severity of COVID-19 (Liu et al., 2020). Our results showed that the serum IL-6 levels in not severely ill and severely ill individuals were 14 ± 5 pg/mL and 66 ± 9 pg/mL, respectively (Figure 1E), which was consistent with the previous report.

To evaluate the accuracy of IFP35 to predict the severity of COVID-19, we obtained the ROC curves of IFP35 and other clinically available biomarkers, including CRP, PCT, TNF, and IL-6. As shown in Figure 1F, the area under the curve of IFP35 is 0.81. The optimal cutoff value of the serum IFP35 concentration is 131.7 pg/mL (sensitivity, 81.93%; specificity, 75.86%), which is comparable with those of CRP and PCT. These results showed that the serum concentrations of IFP35 are correlated with the severity of COVID-19, indicating that IFP35 has potential as a clinical diagnostic marker.

Blood IFP35 is a biomarker of COVID-19

To study the characteristics of blood IFP35 as biomarker of COVID-19, we performed a statistical analysis of the clinical parameters of the 112 individuals with COVID-19 in group 1. First, our binary logistic regression analysis clearly showed that IFP35 was the main factor ($p = 0.001$) associated with the severity of disease (Figure 2A). In addition, we performed principal-component analysis (PCA) to study the correlation between serum levels of IFP35 and disease severity. As shown in Figure 2B and Table S6, two components, PC1 and PC2, are characterized by the largest and second-largest eigenvalues. These two components are responsible for 50.97% of the overall variance. PC1 comprised four main variables (CRP, LDH, IL-6, and neutrophils) and was responsible for 39.06% of total variability. PC2 comprised the main variable IFP35 and was responsible for 11.91% of total variability (Table S7). Furthermore, our Spearman's rank analysis showed that the correlation between IFP35 and age ($r = 0.04$, $p = 0.68$), IL-6 ($r = 0.05$, $p = 0.58$), CRP ($r = 0.13$, $p = 0.19$), and PCT ($r = 0.04$, $p = 0.68$) was not significant (Figures 2C–2F). Thus, our results suggest that IFP35 serves as a biomarker of COVID-19 that is not related to previously reported biomarkers.

Blood IFP35 levels predict the outcome of individuals with COVID-19

To examine whether serum concentrations of IFP35 change during the course of the disease, we conducted a follow-up study by randomly selecting eight individuals with COVID-19 in group 1 and measured the concentrations of IFP35 and IL-6 in their sera before and after treatment (Table S3). Eight individuals who were diagnosed with severe pneumonia on admission had high serum levels of IFP35 and IL-6. After treatment, both IFP35 and IL-6 decreased to a level comparable to those in unifected donors (Figures 3A and 3B). The individuals' condition was also confirmed by chest computed tomography (CT) scanning. Before treatment, we observed multifocal ground-glass opacities around the lungs, especially on the marginal area of the lungs, which is characteristic of COVID-19 infection (Guan et al., 2020; Liu et al., 2020; Zhou et al., 2020a). As shown in Figure 3C, the lung lesions improved considerably after treatment.

Next we analyzed the correlation between IFP35 serum levels and treatment outcome using 38 individuals in group 2 (Table S2). In the sera of 11 deceased individuals in this group, the concentrations of IFP35 reached an average of 4,683 ± 1,233 pg/mL. Notably, 10 of the 11 deceased individuals exhibited serum IFP35 levels ranging from 1,046 pg/mL to 12,435 pg/mL, which was above 950 pg/mL, the average level for severely ill individuals in group 1 (Figure 3D). In contrast, the average level of serum IFP35 in improved individuals was 137 ± 41 pg/mL, which was close to those levels detected in uninfected donors. In contrast to IFP35, IL-6 levels showed no clear correlation with treatment outcome (Figure 3E). These results demonstrate that IFP35 is related to development of disease and may be used as a marker to predict prognosis.

SARS-CoV-2 and influenza virus infection promote release of IFP35 in mouse models

Considering the possibility that clinical individuals are cross-infected with multiple pathogens and various basic diseases, we further studied release of IFP35 upon SARS-CoV-2 infection using human angiotensin-converting enzyme 2 transgenic mice (HFH4-hACE2 in C3B6 mice) (Zhou et al., 2020b). The sera of mice ($n = 5$) were collected 4 days after intranasal inoculation with 5× the median lethal dose ($5LD_{50}$) of SARS-CoV-2 (WIV04). As shown in Figures 4A and 4B, the concentrations of serum mouse interferon-induced protein 35 (mIFP35) and mouse interleukin-6 (mIL-6) in SARS-CoV-2-infected mice reached 819.3 ± 295.5 pg/mL and 137.5 ± 52.89 pg/mL, respectively. In contrast, the average levels of these two proteins in the sera of uninfected hACE2 transgenic mice only reached 102 ± 59.93 pg/mL and 24 ± 1.74 pg/mL. In addition, we studied release of IFP35 in influenza-infected mice. We inoculated C57BL/6J mice ($n = 5$) with $2LD_{50}$ (2×10^6 plaque-forming units [PFUs]) of the A/Puerto Rico/8/1934 (H1N1) virus and collected their sera after infection. We found that the serum concentrations of IFP35 in C57BL/6J mice were constrained at a relatively low level under influenza virus infection within 48 h. They were elevated significantly on the third day and increased gradually over the first 7 days after infection (Figure S1B). The concentrations of mIFP35 and mIL-6 in PR8 infected mice reached 1,024 ± 135 pg/mL and 135.8 ± 11.48 pg/mL 3 days after infection (Figures 4C and 4D). In mock-infected mice, they were only 118 ± 60 pg/mL and 23.69 ± 9.79 pg/mL, respectively. The process of lung damage induced by PR8 was studied using hematoxylin and eosin staining (Figure S1C). These results indicate that SARS-CoV-2 and influenza virus infection result in elevated serum levels of IFP35.

IFP35 has been reported to be released by macrophages stimulated by LPS (Xiahou et al., 2017). However, it remains unclear whether they are released by macrophages or lung epithelial cells during viral infection. Thus, A549 lung epithelial cells and RAW264.7 macrophage were inoculated separately with A/Puerto Rico/8/1934 (H1N1) virus (5 MOI). Phosphate-buffered saline (PBS) and 100 ng/mL LPS were used as negative and positive control, respectively. We found that IFP35 was secreted 3 h after influenza infection (Figure S1A). As shown in Figure 4E, we detected minimal amounts of IFP35 in A549 cell culture medium inoculated with PBS. In contrast, IFP35

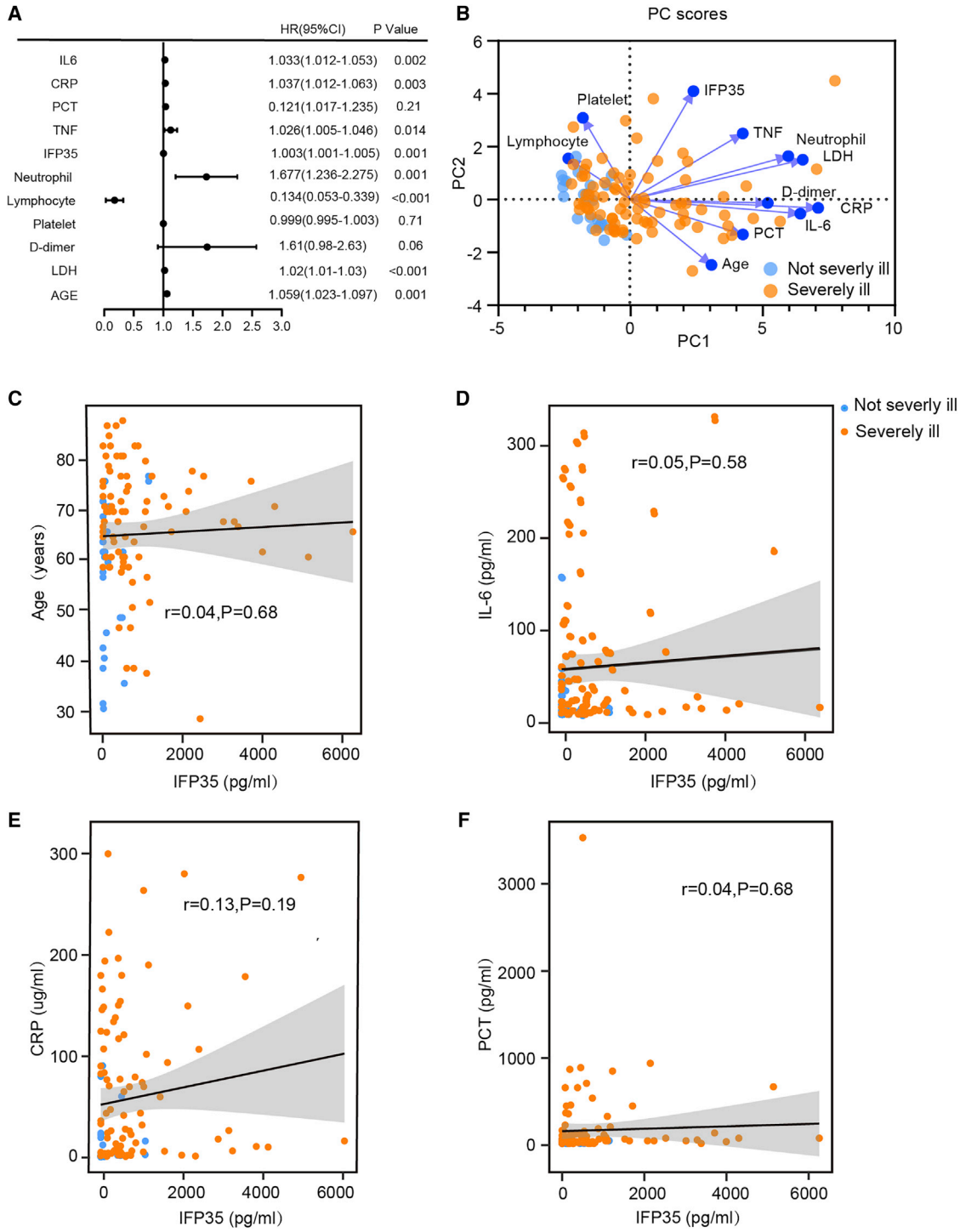

Figure 2. Correlations between serum levels of IFP35 with disease severity and other clinical parameters

(A) Binary logistic regression analyses of clinical parameters associated with disease severity; severely ill cases (n = 83) versus not severely ill cases (n = 29).

(B) Principal-component analysis (PCA) of clinical parameters in 112 individuals with COVID-19. PC1 explains 39.06% of the variation, and PC2 explains 11.91% of the variation. Color denotes disease status (severely ill, n = 83; not severely ill, n = 29).

(C–F) Spearman's correlation analysis of serum level of IFP35 with age (C), IL-6 (D), CRP (E), and PCT (F). Correlations with $r > 0.3$, $r < -0.3$, and $p < 0.01$ were considered significant.

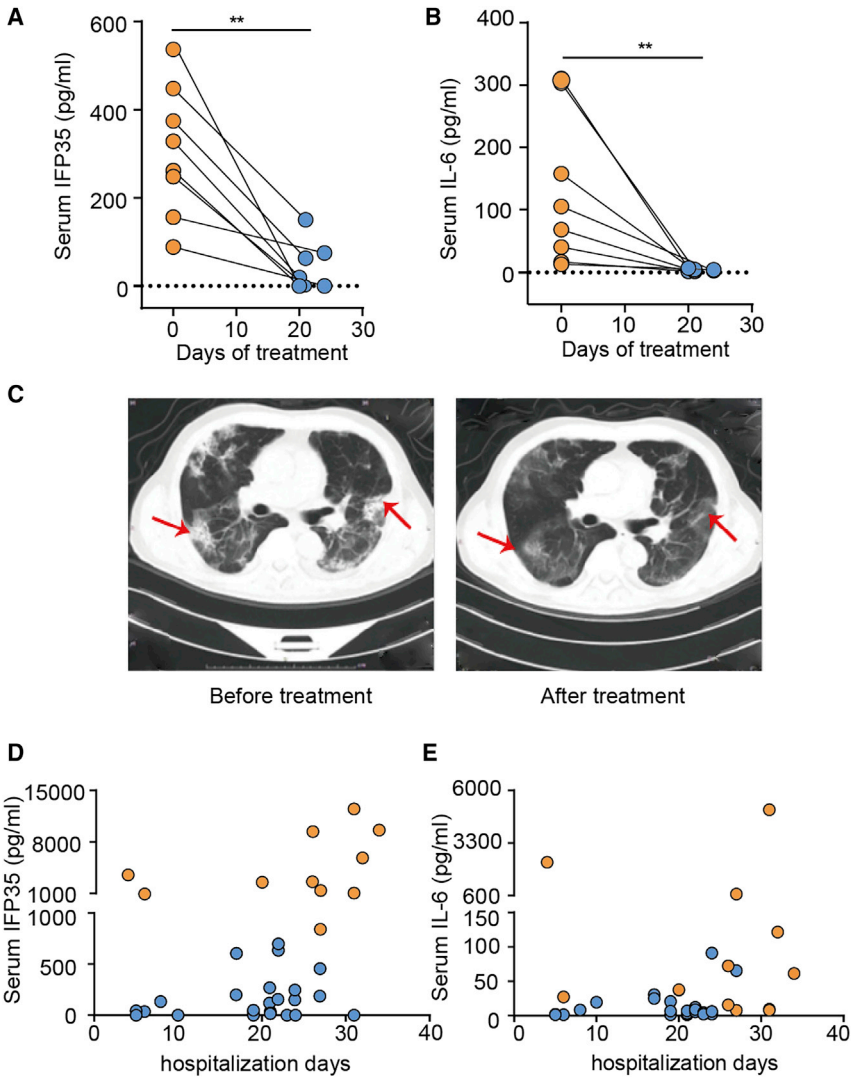

Figure 3. Blood IFP35 reflected the turnover of individuals with COVID-19

(A and B) Serum IFP35 (A) and IL-6 (B) in 8 severely ill individuals with COVID-19 before and after treatment. Significance was calculated by two-tailed Wilcoxon matched-pairs signed rank test (*$p < 0.05$, **$p < 0.01$).

(C) Chest computed tomography (CT) in a severely ill individual with COVID-19 before and after treatment. The bilateral, multiple, patchy, ground-glass opacities before treatment are indicated by red arrows and were located in the same position after treatment when the lesions were improved.

(D and E) IFP35 (D) and IL-6 (E) in the sera of individuals in group 2. Data from 11 deceased individuals and 26 improved individuals are shown as orange dots and blue dots, respectively.

increased up to 2,378 ± 339 pg/mL 6 h after infection and rose to 3,588 ± 20 pg/mL 12 h after infection. We obtained similar results when using mouse macrophage RAW264.7 cells infected with influenza virus (Figure 4F). A549 human lung epithelial cells and RAW264.7 mouse macrophages released IFP35 protein upon influenza virus infection.

The pro-inflammatory action of IFP35 in an influenza-infected mouse model

We speculated that released IFP35 enhances the inflammatory response during virus infection. To test this hypothesis, we built an influenza virus-induced sepsis model by inoculating mice intranasally with $2LD_{50}$ of PR8 virus. A group of 8-week-old *Ifp35*$^{-/-}$ mice was studied using age- and sex-matched C57BL/6J wild-type mice as a control. Wild-type and knockout mice infected with influenza virus developed symptoms of pneumonia. The mice were then monitored daily for survival, weight loss, and clinical signs of illness (*e.g.* lethargy, piloerection, ruffled fur, hunched posture, rapid shallow breathing, and audible crackling) for 14 days. A clinical score ranging from 0 (no symptoms) to 5 (death or moribund) was recorded daily for each mouse according to a previous study (Shirey et al., 2013).

The body weight of *Ifp35*$^{-/-}$ and wild-type mice reached the lowest value 7 and 8 days after infection. The average body weight of wild-type and *Ifp35*$^{-/-}$ mice decreased to 76.03% and 72.2% of that before infection, respectively (Figure 5A). In contrast with a limited difference in body weight loss, *Ifp35*$^{-/-}$ mice showed mild clinical symptoms, as indicated by clinical scores in the first week after PR8 infection (Figure 5B). According to the clinical score, *Ifp35* knockout delayed the peak incidence of mice from day 7 to day 9. At the most severe stage, the clinical score of wild-type mice was 4.22 (day 7), whereas the clinical score of *Ifp35*$^{-/-}$ mice was 3.05 (day 9). The survival rate of *Ifp35*$^{-/-}$ mice was 50% (6 of 12), which was higher than that of wild-type mice (25%, 3 of 12) (Figure 5C).

To inspect lung injury caused by influenza virus, we performed hematoxylin and eosin (H&E) staining of the lung tissues collected on day 3. As shown in Figure 5D, the lung tissue of wild-type mice was damaged severely following infection with influenza virus. The alveolar space and alveolar septum were filled with fibrin exudation. Lymphocyte and macrophage infiltration was observed in multifocal lesions. Accumulation of these inflammatory cells in the alveolar interstitium caused thickening of the alveolar walls. In contrast, the lung tissue of *Ifp35*$^{-/-}$ mice appeared to remain largely intact after infection, with only a small amount of fibrin exudation detectable in the alveolar space. Bronchial epithelial cells were slightly degenerated and desquamated. The lung tissue of PBS-inoculated *Ifp35*$^{-/-}$ mice was intact, and no lesions were observed. This appearance was similar to that of PBS-inoculated C57BL/6J wild-type mice (healthy controls). The pathological score of lung tissue in *Ifp35*$^{-/-}$

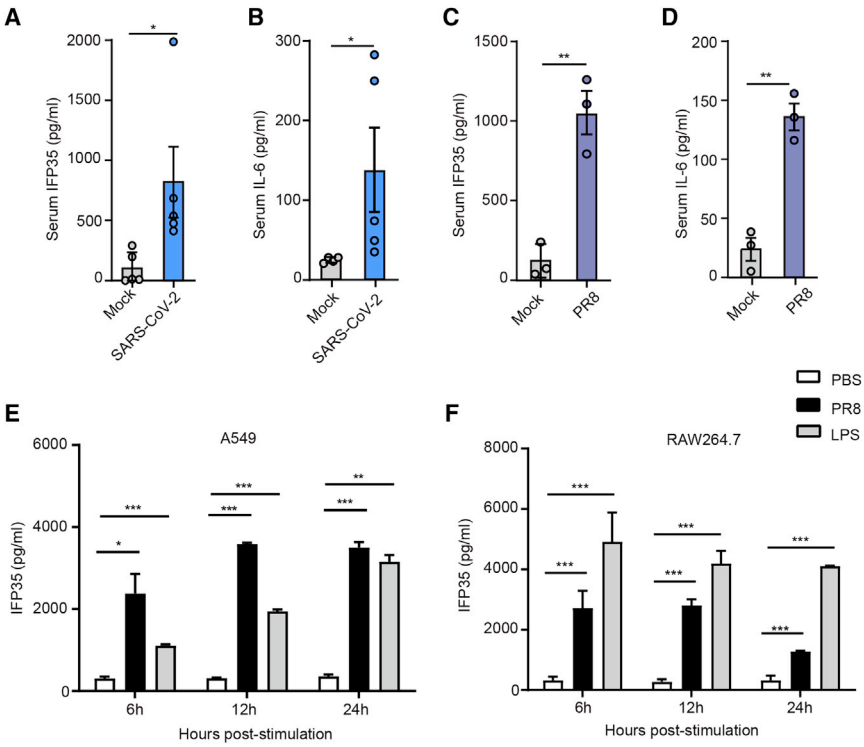

Figure 4. IFP35 was released *in vitro* and *in vivo* upon virus infection

(A and B) IFP35 (A) and IL-6 (B) in the sera of hACE2 mice 4 days after SARS-CoV-2 ($5LD_{50}$, 1.5×10^5 tissue culture infectious dose 50 [$TCID_{50}$]/50 μL) infection; n = 5.

(C and D) IFP35 (C) and IL-6 (D) in the sera of C57BL/6J mice 3 days after PR8 ($2LD_{50}$, 2×10^6 PFU) infection; n = 3.

(E and F) IFP35 released by A549 (E) and RAW264.7 (F) cells, stimulated by PR8 (5 MOI). LPS (100 ng/mL) and PBS were used as positive and negative control, respectively.

Data are mean values ± SEM. Significance in (A)–(D) was analyzed using unpaired Student's t test. Significance of (E) and (F) was conducted by multiple-comparisons one-way analysis of variance (ANOVA). *p < 0.05, **p < 0.01, ***p < 0.001.

mice decreased significantly ($p < 0.01$) compared with that of wild-type mice (Figure 5E). Next we measured the concentrations of TNF and IL-6 in the sera of influenza virus-infected mice. Our results showed that the mean values of serum TNF and IL-6 in wild-type mice were 578 ± 63 pg/mL and 255 ± 105 pg/mL, higher than that in *Ifp35*$^{-/-}$ mice with 377 ± 39 pg/mL ($p < 0.01$) and 67 ± 11 pg/mL ($p < 0.01$), respectively (Figures 5F and 5G).

Because *Ifp35*$^{-/-}$ alleviated clinical symptoms and protected the host from lethal influenza virus infection, we investigated whether these effects were due to antiviral activity in *Ifp35*$^{-/-}$ mice. We determined the replication levels of the progeny influenza virus in mice using quantitative reverse-transcriptase polymerase chain reaction (qRT-PCR). As shown in Figure 5H, we found that the mean values of viral genome RNA (vRNA) ($\log_{10}^{(\text{vRNA copies/g})}$) in wild-type and *Ifp35*$^{-/-}$ mice reached 7.83 and 8.31, respectively. Because there was little significant difference in the values of viral genome RNA ($p = 0.1797$) between *Ifp35*$^{-/-}$ and the wild-type groups, we concluded that the protective effects of knockout resulted from inhibition of the pro-inflammatory response rather than from virus replication. Our results are in agreement with a previous report showing that *Ifp35* deficiency causes reduced morbidity in mouse models of highly pathogenic H5N1 and pandemic H1N1 influenza virus infection by decreasing production of specific cytokines and chemokines but not affecting virus replication (Gounder et al., 2018).

Anti-IFP35 protects mice from SARS-CoV-2 and influenza virus infection

To study whether released IFP35 exacerbated the severity of the inflammatory response, we developed a neutralizing antibody against IFP35 (anti-IFP35). The activity of the antibody was tested in SARS-CoV-2- and influenza virus-induced sepsis models, using a mouse immunoglobulin G (mIgG) as a negative control.

We developed a severe sepsis model by infecting mice with $2LD_{50}$ of PR8 virus. The process of the influenza virus infected mouse model is shown in Figure 6A. Briefly, on day −1, 1 day prior to virus infection, 8-week-old C57BL/6J mice in the testing group (n = 12) and control group (n = 12) were injected intravenously with 200 μg anti-IFP35 and 200 μg mIgG, respectively. The mice were inoculated intranasally with 2 LD_{50} of PR8 virus on day 0. The mice were administered the corresponding antibody daily for 5 successive days. Each mouse was weighed, and the clinical symptoms mentioned above were scored daily for 2 weeks. As shown in Figures 6B and 6C, mice treated with anti-IFP35 showed mild symptoms with lower clinical scores throughout the 14 days after infection compared with mIgG-treated mice, although their body weight loss failed to improve. At the end of the experiment, 75% (9 of 12) of the mice in testing group survived, whereas 25% (3 of 12) of the mice treated with mIgG survived (Figure 6D). H&E staining showed that the lung tissue of virus-infected positive control and mIgG-treated mice was damaged severely and lost the whole structure. The alveolar space and alveolar septum were merged and filled with fibrin exudation, lymphocyte and macrophage infiltration, and hyaline membrane formation. However, the lung tissue of anti-IFP35-treated mice remained largely intact, although we still detected multifocals with collagen fibrin exudation, inflammatory cell infiltration, and thickened alveolar walls (Figure 6E). The pathological score of lung tissue in anti-IFP35-treated mice decreased significantly ($p < 0.01$) compared with that of mIgG-treated mice (Figure 6F). Furthermore, the serum TNF level in anti-IFP35-treated mice was 221 ± 7 pg/mL, a significant decrease ($p < 0.01$) compared with 356 ± 42 pg/mL in mIgG-treated mice (Figure 6G). However, we failed to detect a significant difference in the number of viral genome RNA copies between each group of mice,

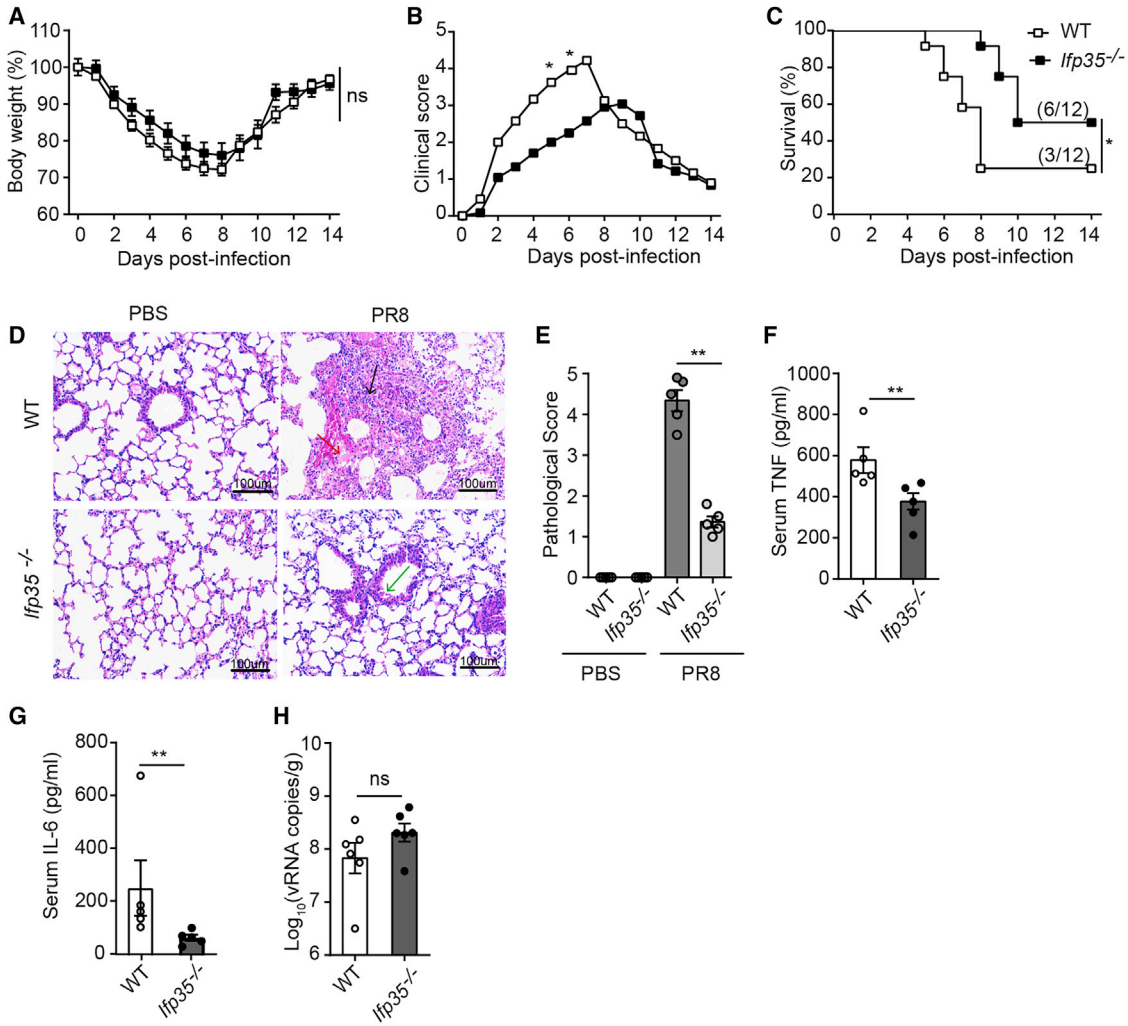

Figure 5. *Ifp35*$^{-/-}$ mice have attenuated clinical symptoms after lethal influenza virus infection

(A–C) Body weight loss (percent) (A), clinical score (B), and survival rate (percent) (C) of C57BL/6J wild-type mice and *Ifp35*$^{-/-}$ mice infected with PR8 ($2LD_{50}$); n = 12.

(D) H&E staining of the lung tissue. Lymphocyte and macrophage infiltration in the multifocal lesions is indicated by black arrow. Fibrin exudation in the alveolar space and alveolar septum is indicated by a red arrow. Degenerative and desquamated bronchial epithelial cells are indicated by a green arrow. Scale bars, 100 μm. The picture is shown as original magnifications ×100.

(E) The pathological score of the lung tissue in *Ifp35*$^{-/-}$ mice.

(F and G) Serum TNF and IL-6 (pg/mL) in mice 3 days after PR8 infection, detected by ELISA; n = 5.

(H) qRT-PCR results of PR8 viral genome RNA (nucleoprotein, NP) in the lung tissue of C57BL/6J wild-type mice and *Ifp35*$^{-/-}$ mice 3 days after infection; n = 6.

Data in (E)–(H) are mean values ± SEM. Significance in (A) and (B) was calculated with two-way ANOVA with Sidak's post-test. Significance in (C) was determined using log rank test. Significance in (E)–(H) was assessed by Mann-Whitney *U* test. *p < 0.05,**p < 0.01, ***p < 0.001; ns, no significance.

suggesting that anti-IFP35 minimally affected progeny virus replication (Figure 6H).

Next we investigated the function of anti-IFP35 in COVID-19, which was induced by an extremely high dose ($5LD_{50}$) of SARS-CoV-2. 24 8-week-old hACE2 male mice were divided randomly into testing and control groups. As shown in Figure 7A, on day 0, each mouse was inoculated intranasally with $5LD_{50}$ of SARS-CoV-2, which was determined to kill 100% of mice within 10 days. 24 h later, anti-IFP35 was administered daily intraperitoneally (i.p.) (250 μg per mouse from day 1 to day 3). 12 h later, anti-IFP35 was administered every 12 h for 5 consecutive days (250 μg per mouse from day 3.5 to day 8) (Figure 7A). Each mouse was weighed and scored daily for 2 weeks. In this SARS-CoV-2-induced sepsis model, all mice administered mIgG died within 10 days (Figure 7B). In addition, mice treated with mIgG showed severe clinical symptoms with a clinical score of 5 from day 6. These severe clinical symptoms improved little in the late stages of infection (Figure 7C). In this critical case, anti-IFP35 still protected 25% of mice (3 of 12) from SARS-CoV-2-induced lethality during the 14-day period (Figure 7D). This result was consistent with the reduced body weight loss and clinical scores of anti-IFP35-treated mice

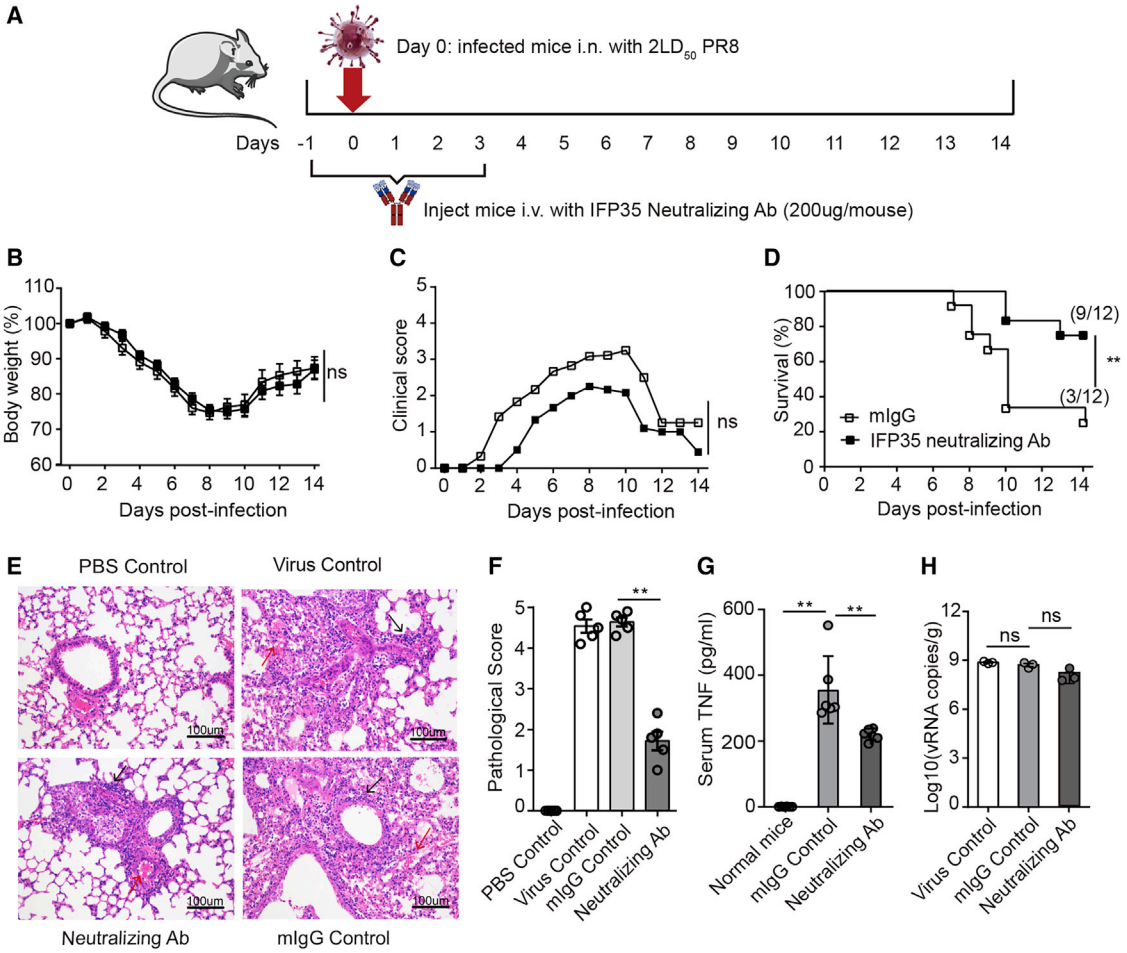

Figure 6. Anti-IFP35 protected C57BL/6J mice from lethal influenza virus infection

(A) Schematic of the experimental protocol using anti-IFP35 against influenza infection.

(B–D) Body weight loss (percent) (B), clinical score (C), and survival rate (percent) (D) of anti-IFP35- or mIgG-treated mice under 2 × 10^6 PFU PR8 virus infection; n = 12.

(E) H&E staining of the lung tissue. Scale bars, 100 μm. Multifocals with collagen fibrin exudation are indicated by a red arrow. Inflammatory cells are indicated by a black arrow.

(F) The pathological score of the lung tissue in anti-IFP35-treated mice decreased.

(G) Serum TNF in anti-IFP35- or mIgG-treated mice infected with $2LD_{50}$ PR8 virus.

(H) PR8 viral genome RNA (nucleoprotein, NP) in the lung tissue of C57BL/6J mice; n = 3.

Data in (F)–(H) are mean values ± SEM. Significance in (B) and (C) was calculated with two-way ANOVA with Sidak's post-test. Significance in (D) was determined using log rank test (*p < 0.05, **p < 0.01). Significance in (F)–(H) was assessed by Mann-Whitney *U* test (*p < 0.05, **p < 0.01, ***p < 0.001; ns, no significance).

from day 6 after infection (Figures 7B and 7C). We also found that the lung tissue of mIgG-injected control mice or virus-infected control mice was damaged and lost its structure. However, the lung tissue of anti-IFP35-treated hACE2 mice remained intact, with no visible lesions, and the appearance of the alveoli was similar to those of PBS-inoculated control mice (Figure 7E). The pathological score of lung tissue in anti-IFP35-treated mice decreased significantly ($p < 0.01$) compared with that of mIgG-treated mice (Figure 7F). Furthermore, we failed to detect any significant difference for viral genome RNA copies between the different groups, suggesting that anti-IFP35 minimally affected progeny virus replication (Figure 7G). Our results demonstrated that anti-IFP35 alleviated the clinical symptoms and protected the mice from lethal SARS-CoV-2 or influenza virus infection, although the efficiency is different for these two syndromes.

DISCUSSION

Here we identified IFP35 as a promising biomarker and therapeutic target for the syndromes induced by SARS-CoV-2 or influenza virus. Our result showed that serum IFP35 increased in individuals with COVID-19, especially in severe cases. In addition, we found that IFP35 was released by macrophages and lung epithelial cells after SARS-CoV-2 or influenza virus infection. Administration of IFP35 neutralizing antibodies remarkably

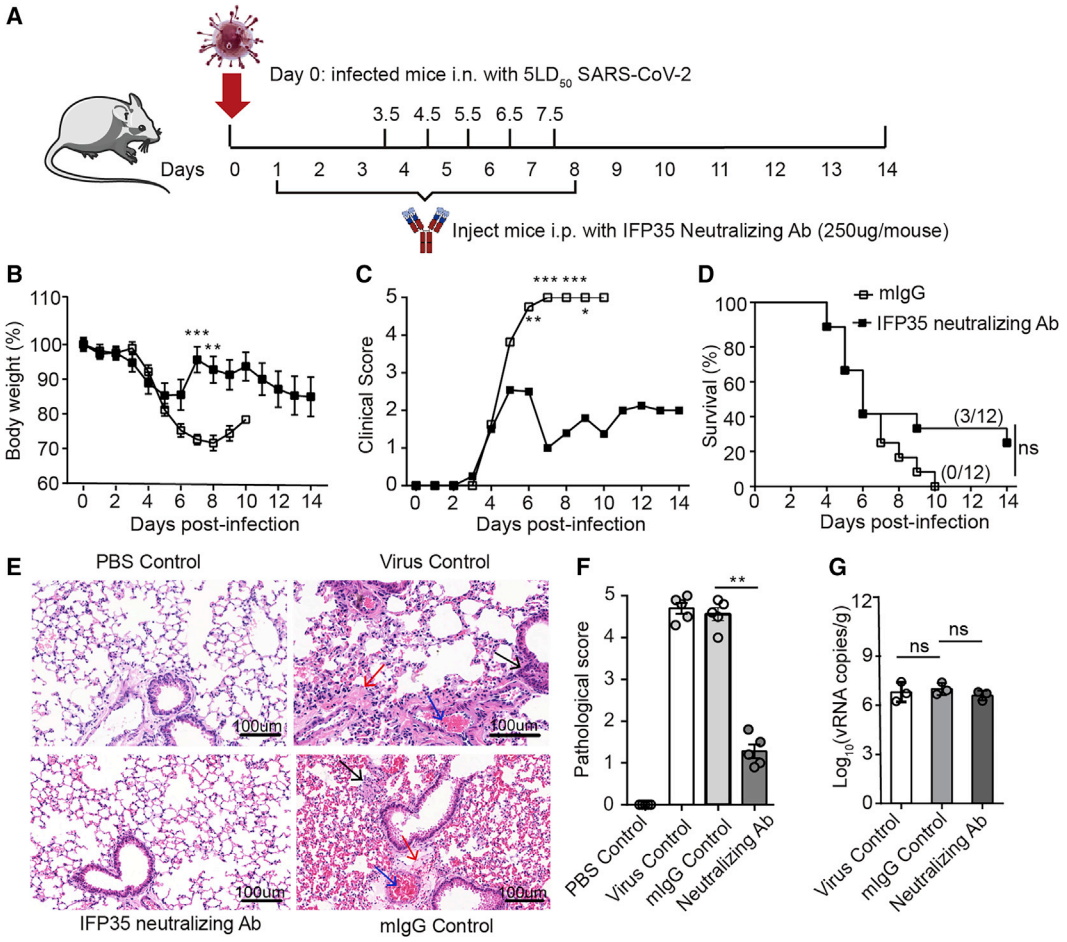

Figure 7. Anti-IFP35 protected hACE2 mice from lethal SARS-CoV-2 infection

(A) Schematic of the experimental protocol using anti-IFP35 against SARS-CoV-2 infection.

(B–D) Body weight loss (percent) (B), clinical score (C), and survival rate (percent) (D) of anti-IFP35- or mIgG-treated mice under $5LD_{50}$ (1.5×10^5 $TCID_{50}$/50 μL) SARS-CoV-2 infection; n = 12.

(E) H&E staining of the lung tissue. Scale bars, 100 μm. Inflammatory cells, fibrin exudation, and red blood cells blocked in the blood vessel are indicated by black, red, and blue arrows, respectively.

(F) The pathological score of the lung tissue in anti-IFP35-treated mice.

(G) SARS-CoV-2 viral genome RNA (S gene) in the lung tissue of hACE2 mice 4 days after SARS-CoV-2 infection ($5LD_{50}$); n = 3.

Data in (F and G) are mean values ± SEM. Significance in (B) and (C) was calculated with two-way ANOVA with Sidak's post-test. Significance in (D) was determined using log rank test. Significance in (F) and (G) was assessed by Mann-Whitney *U* test. *p < 0.05, **p < 0.01, ***p < 0.001; ns, no significance.

alleviated severe pneumonia and reduced the fatality rate in SARS-CoV-2- or influenza-infected mice.

We showed that the content of IFP35 in serum was correlated positively with the condition of individuals infected with SARS-CoV-2. Compared with the extensively used biomarkers in the clinic, including CRP and PCT, IFP35 showed a comparable prediction ability for the severity of COVID-19. Importantly, our results showed that IFP35 has a better predictive ability for the outcome of severely ill individuals than IL-6, which is currently used as a clinical biomarker of excessive inflammation in COVID-19 (Del Valle et al., 2020). We speculate that the reason might be that IL-6 reflects the level of the inflammatory response, whereas IFP35 directly reflects the level of cellular and tissue damage. Our PCA and Spearman's rank correlation analysis also showed that IFP35 is a kind of biomarker. For example, the Spearman's rank correlation analysis results showed that the serum content of IFP35 in individuals with COVID-19 does not correlate well with CRP, PCT, or IL-6 levels. We propose that combined application of IFP35 with other biomarkers might enable a more accurate diagnosis of the severity of an individual's condition.

We also found that IFP35 may serve as a therapeutic target in severe COVID-19 and influenza infection. Although many immunomodulatory drugs targeting specific cytokines, such as IL-6 and TNF antibodies, are available, there is no reliable clinical study that confirms their effectiveness in treatment of COVID-19. Our results showed that anti-IFP35 was effective in treating the viral infection, at least in the animal model. We observed that the therapeutic effect of IFP35 in severe influenza infection was comparable with that of inhibitors of the S1P1 receptor,

one of the most promising target of immunotherapy for influenza infection so far (Jia et al., 2018; Khalili et al., 2018; Oldstone et al., 2013). In the SARS-CoV-2-infected mouse model, anti-IFP35 treatment saved 25% of the mice even with an extremely high viral load. Because IFP35 can be detected at the early stage of viral infection, early treatment is available to control the development of excessive inflammatory responses.

Although it has been reported that the mRNA and protein levels of TLR-4 increased under influenza virus infection (Dai et al., 2017, 2018), there are controversial data and discussions regarding the role of TLR-4 signaling in influenza infection, whether it is beneficial or detrimental for survival (Shinya et al., 2011; Shirey et al., 2013). However, the function of TLR-4 is defined more clearly in COVID-19. First, our results showed that most of our individuals with COVID-19 have elevated PCT, which indicates that they have secondary bacterial infections. In addition, it has been reported recently that the SARS-CoV-2 spike protein interacts with TLR-4, provoking an anti-bacterial-like response at the very early stage of infection (Zhao et al., 2021). More importantly, our previous studies showed that IFP35 triggers the NF-κB signaling pathway and upregulates the inflammation response through TLR-4 (Xiahou et al., 2017). Therefore, we speculate that downregulated TLR-4 will be beneficial for individuals with COVID-19.

Although our results showed that IFP35 possesses a number of clinical strengths, the present study still has many questions that should be addressed. For example, we found exceptions where some severely ill individuals (15 of 83) have low serum IFP35. Because IFP35 in severely ill individuals is mostly released passively by dying cells, we speculated that serum IFP35 in these severely ill individuals may be degraded by various serum proteases in the bloodstream because these individuals have serious organ impairment. Thus, the stability of blood IFP35 requires further investigation. In addition, elderly people are at high risk for influenza- and SARS-CoV-2-related morbidity and mortality. For example, Samy and Lim (2015) claimed that "ageing is associated with increased pro-inflammatory cytokine production and as a result, lung inflammation is often present in elderly people." Although we did not observe a wide range of IFP35 increases in uninfected elderly people, we did not avoid false negative results limited by the low sensitivity of the currently available ELISA kit. Furthermore, we did not conduct an in-depth investigation of the rational therapeutic schedule for administration of IFP35 antibodies. Finally, we reported that N-myc and STAT interactor (NMI), the homologous protein of IFP35, also functions as pro-inflammatory DAMP during bacterial infection (Xiahou et al., 2017). The role of NMI in influenza and SARS-CoV-2 is still unclear. The differences and crosstalk between NMI and IFP35 need to be studied.

Our results demonstrate that IFP35 is a promising target for clinical diagnosis and treatment in severe influenza and SARS-CoV-2 infection, providing a host factor deserving close attention in other emerging viral infectious diseases.

Limitations of the study

IFP35 was identified as a promising biomarker and as a therapeutic target during SARS-CoV-2 and influenza virus infection. However, the therapeutic effects of a neutralizing antibody against IFP35 were only determined in SARS-CoV-2- and influenza virus-infected mouse models. They need to be determined for treatment of affected individuals.

STAR★METHODS

Detailed methods are provided in the online version of this paper and include the following:

- KEY RESOURCES TABLE
- RESOURCE AVAILABILITY
  - Lead contact
  - Materials availability
  - Data and code availability
- EXPERIMENTAL MODEL AND SUBJECT DETAILS
  - Cell Lines
  - Virus Strain
  - Mice
  - Human Blood Samples
  - Diagnosis and classification of patients
  - Ethics Statement
- METHOD DETAILS
  - Reagents
  - Anti-IFP35 preparation and activity test
  - ELISA
  - Cell stimulation
  - Viral genome RNA determination
  - Lung Tissues Histopathology
- QUANTIFICATION AND STATISTICAL ANALYSIS

SUPPLEMENTAL INFORMATION

Supplemental information can be found online at https://doi.org/10.1016/j.celrep.2021.110126.

ACKNOWLEDGMENTS

We thank Dr. Jin-hui Gu for valuable advice, Prof. Liguo Zhang's lab for preparation of the neutralizing antibody, Prof. Wei Tian's lab for preparation of the gene knockout mice, and Dr. Raph S. Baric from the University of North Carolina for his support and HFH4-hACE2 mice. This work was supported by the National Natural Science Foundation of China (31870739 and 82071346), the "Pearl River Talent Plan" Innovation and Entrepreneurship Team Project of Guangdong Province (2019ZT08Y464), the Natural Science Foundation of Guangdong Province, China (2020B1515020035), the Key Fundamental Research Projects of Shenzhen Science and Technology Plan (JCYJ20200109142418595), and the Guangdong Specific Project for the Control of Novel Coronavirus (2020A111128023).

AUTHOR CONTRIBUTIONS

Y.F.L. and H.H.L. originated the hypothesis and designed the research. Y.Y., N.X., Q.C., F.D., M.L., A.Z., Y.-Q.M., D.Z., W.H., X.F., X.J., Y.C., D.Y., Y.F., C.S., and Q.G. performed the experiments. Z.Y., Jincun Zhao, and W.S. provided help during the animal experiments. Y.Y., N.X., H. Liang, and Y.L. analyzed the data and wrote the manuscript. D.G., H. Liu, Jindong Zhao, P.L., Z.S., and X.C. reviewed the manuscript.

DECLARATION OF INTERESTS

The authors declare no competing interests.

Received: December 31, 2020
Revised: July 30, 2021
Accepted: November 22, 2021
Published: December 3, 2021

REFERENCES

Arabi, Y.M., Mandourah, Y., Al-Hameed, F., Sindi, A.A., Almekhlafi, G.A., Hussein, M.A., Jose, J., Pinto, R., Al-Omari, A., Kharaba, A., et al.; Saudi Critical Care Trial Group (2018). Corticosteroid Therapy for Critically Ill Patients with Middle East Respiratory Syndrome. Am. J. Respir. Crit. Care Med. *197*, 757–767.

Belongia, E.A., and Osterholm, M.T. (2020). COVID-19 and flu, a perfect storm. Science *368*, 1163.

Bosmann, M., and Ward, P.A. (2013). The inflammatory response in sepsis. Trends Immunol. *34*, 129–136.

Buszko, M., Park, J.H., Verthelyi, D., Sen, R., Young, H.A., and Rosenberg, A.S. (2020). The dynamic changes in cytokine responses in COVID-19: a snapshot of the current state of knowledge. Nat. Immunol. *21*, 1146–1151.

Cicco, S., Cicco, G., Racanelli, V., and Vacca, A. (2020). Neutrophil Extracellular Traps (NETs) and Damage-Associated Molecular Patterns (DAMPs): Two Potential Targets for COVID-19 Treatment. Mediators Inflamm. *2020*, 7527953.

Dai, J.P., Wang, Q.W., Su, Y., Gu, L.M., Zhao, Y., Chen, X.X., Chen, C., Li, W.Z., Wang, G.F., and Li, K.S. (2017). Emodin Inhibition of Influenza A Virus Replication and Influenza Viral Pneumonia via the Nrf2, TLR4, p38/JNK and NF-kappaB Pathways. Molecules *22*, 1754.

Dai, J.P., Wang, Q.W., Su, Y., Gu, L.M., Deng, H.X., Chen, X.X., Li, W.Z., and Li, K.S. (2018). Oxymatrine Inhibits Influenza A Virus Replication and Inflammation via TLR4, p38 MAPK and NF-κB Pathways. Int. J. Mol. Sci. *19*, 965.

De Luca, G., Cavalli, G., Campochiaro, C., Della-Torre, E., Angelillo, P., Tomelleri, A., Boffini, N., Tentori, S., Mette, F., Farina, N., et al. (2020). GM-CSF blockade with mavrilimumab in severe COVID-19 pneumonia and systemic hyperinflammation: a single-centre, prospective cohort study. Lancet Rheumatol. *2*, e465–e473.

Del Valle, D.M., Kim-Schulze, S., Huang, H.H., Beckmann, N.D., Nirenberg, S., Wang, B., Lavin, Y., Swartz, T.H., Madduri, D., Stock, A., et al. (2020). An inflammatory cytokine signature predicts COVID-19 severity and survival. Nat. Med. *26*, 1636–1643.

Delaney, J.W., Pinto, R., Long, J., Lamontagne, F., Adhikari, N.K., Kumar, A., Marshall, J.C., Cook, D.J., Jouvet, P., Ferguson, N.D., et al.; Canadian Critical Care Trials Group H1N1 Collaborative (2016). The influence of corticosteroid treatment on the outcome of influenza A(H1N1pdm09)-related critical illness. Crit. Care *20*, 75.

Feldman, A.T., and Wolfe, D. (2014). Tissue processing and hematoxylin and eosin staining. Methods Mol. Biol. *1180*, 31–43.

Florescu, D.F., and Kalil, A.C. (2014). The complex link between influenza and severe sepsis. Virulence *5*, 137–142.

Gokhale, Y., Mehta, R., Kulkarni, U., Karnik, N., Gokhale, S., Sundar, U., Chavan, S., Kor, A., Thakur, S., Trivedi, T., et al. (2021). Tocilizumab improves survival in severe COVID-19 pneumonia with persistent hypoxia: a retrospective cohort study with follow-up from Mumbai, India. BMC Infect. Dis. *21*, 241.

Gong, T., Liu, L., Jiang, W., and Zhou, R. (2020). DAMP-sensing receptors in sterile inflammation and inflammatory diseases. Nat. Rev. Immunol. *20*, 95–112.

Gostin, L.O., and Salmon, D.A. (2020). The Dual Epidemics of COVID-19 and Influenza: Vaccine Acceptance, Coverage, and Mandates. JAMA *324*, 335–336.

Gounder, A.P., Yokoyama, C.C., Jarjour, N.N., Bricker, T.L., Edelson, B.T., and Boon, A.C.M. (2018). Interferon induced protein 35 exacerbates H5N1 influenza disease through the expression of IL-12p40 homodimer. PLoS Pathog. *14*, e1007001.

Grodzki, A.C., and Berenstein, E. (2010). Antibody purification: affinity chromatography - protein A and protein G Sepharose. Methods Mol. Biol. *588*, 33–41.

Guan, W.J., Ni, Z.Y., Hu, Y., Liang, W.H., Ou, C.Q., He, J.X., Liu, L., Shan, H., Lei, C.L., Hui, D.S.C., et al.; China Medical Treatment Expert Group for Covid-19 (2020). Clinical Characteristics of Coronavirus Disease 2019 in China. N. Engl. J. Med. *382*, 1708–1720.

Harris, H.E., and Raucci, A. (2006). Alarmin(g) news about danger: workshop on innate danger signals and HMGB1. EMBO Rep. *7*, 774–778.

Hoffmann, E., Neumann, G., Kawaoka, Y., Hobom, G., and Webster, R.G. (2000). A DNA transfection system for generation of influenza A virus from eight plasmids. Proc. Natl. Acad. Sci. USA *97*, 6108–6113.

Hornbeck, P.V. (2015). Enzyme-Linked Immunosorbent Assays. Curr. Protoc. Immunol. *110*, 2.1.1–2.1.23.

Hou, Y.J., Chiba, S., Halfmann, P., Ehre, C., Kuroda, M., Dinnon, K.H., 3rd, Leist, S.R., Schäfer, A., Nakajima, N., Takahashi, K., et al. (2020). SARS-CoV-2 D614G variant exhibits efficient replication ex vivo and transmission in vivo. Science *370*, 1464–1468.

Jia, X., Liu, B., Bao, L., Lv, Q., Li, F., Li, H., An, Y., Zhang, X., Cao, B., and Wang, C. (2018). Delayed oseltamivir plus sirolimus treatment attenuates H1N1 virus-induced severe lung injury correlated with repressed NLRP3 inflammasome activation and inflammatory cell infiltration. PLoS Pathog. *14*, e1007428.

Jiang, R.D., Liu, M.Q., Chen, Y., Shan, C., Zhou, Y.W., Shen, X.R., Li, Q., Zhang, L., Zhu, Y., Si, H.R., et al. (2020). Pathogenesis of SARS-CoV-2 in Transgenic Mice Expressing Human Angiotensin-Converting Enzyme 2. Cell *182*, 50–58.e8.

Khalili, N., Karimi, A., Moradi, M.T., and Shirzad, H. (2018). In vitro immunomodulatory activity of celastrol against influenza A virus infection. Immunopharmacol. Immunotoxicol. *40*, 250–255.

Land, W.G. (2021). Role of DAMPs in respiratory virus-induced acute respiratory distress syndrome-with a preliminary reference to SARS-CoV-2 pneumonia. Genes Immun. *22*, 141–160.

Liu, T., Zhang, J., Yang, Y., Ma, H., Li, Z., Zhang, J., Cheng, J., Zhang, X., Zhao, Y., Xia, Z., et al. (2020). The role of interleukin-6 in monitoring severe case of coronavirus disease 2019. EMBO Mol. Med. *12*, e12421.

Luo, P., Liu, Y., Qiu, L., Liu, X., Liu, D., and Li, J. (2020). Tocilizumab treatment in COVID-19: A single center experience. J. Med. Virol. *92*, 814–818.

Mulchandani, R., Lyngdoh, T., and Kakkar, A.K. (2021). Deciphering the COVID-19 cytokine storm: Systematic review and meta-analysis. Eur. J. Clin. Invest. *51*, e13429.

Oldstone, M.B., Teijaro, J.R., Walsh, K.B., and Rosen, H. (2013). Dissecting influenza virus pathogenesis uncovers a novel chemical approach to combat the infection. Virology *435*, 92–101.

Patel, M.C., Shirey, K.A., Boukhvalova, M.S., Vogel, S.N., and Blanco, J.C.G. (2018). Serum High-Mobility-Group Box 1 as a Biomarker and a Therapeutic Target during Respiratory Virus Infections. MBio *9*, e00246-18.

Petrova, V.N., and Russell, C.A. (2018). The evolution of seasonal influenza viruses. Nat. Rev. Microbiol. *16*, 60.

Salama, C., Han, J., Yau, L., Reiss, W.G., Kramer, B., Neidhart, J.D., Criner, G.J., Kaplan-Lewis, E., Baden, R., Pandit, L., et al. (2021). Tocilizumab in Patients Hospitalized with Covid-19 Pneumonia. N. Engl. J. Med. *384*, 20–30.

Samy, R.P., and Lim, L.H. (2015). DAMPs and influenza virus infection in ageing. Ageing Res. Rev. *24* (*Pt A*), 83–97.

Shinde, V., Bhikha, S., Hoosain, Z., Archary, M., Bhorat, Q., Fairlie, L., Lalloo, U., Masilela, M.S.L., Moodley, D., Hanley, S., et al.; 2019nCoV-501 Study Group (2021). Efficacy of NVX-CoV2373 Covid-19 Vaccine against the B.1.351 Variant. N. Engl. J. Med. *384*, 1899–1909.

Shinya, K., Okamura, T., Sueta, S., Kasai, N., Tanaka, M., Ginting, T.E., Makino, A., Eisfeld, A.J., and Kawaoka, Y. (2011). Toll-like receptor pre-stimulation protects mice against lethal infection with highly pathogenic influenza viruses. Virol. J. *8*, 97.

Shirey, K.A., Lai, W., Scott, A.J., Lipsky, M., Mistry, P., Pletneva, L.M., Karp, C.L., McAlees, J., Gioannini, T.L., Weiss, J., et al. (2013). The TLR4 antagonist Eritoran protects mice from lethal influenza infection. Nature *497*, 498–502.

Soin, A.S., Kumar, K., Choudhary, N.S., Sharma, P., Mehta, Y., Kataria, S., Govil, D., Deswal, V., Chaudhry, D., Singh, P.K., et al. (2021). Tocilizumab plus standard care versus standard care in patients in India with moderate to severe COVID-19-associated cytokine release syndrome (COVINTOC): an open-label, multicentre, randomised, controlled, phase 3 trial. Lancet Respir. Med. *9*, 511–521.

Song, J.W., Zhang, C., Fan, X., Meng, F.P., Xu, Z., Xia, P., Cao, W.J., Yang, T., Dai, X.P., Wang, S.Y., et al. (2020). Immunological and inflammatory profiles in mild and severe cases of COVID-19. Nat. Commun. *11*, 3410.

Stone, J.H., Frigault, M.J., Serling-Boyd, N.J., Fernandes, A.D., Harvey, L., Foulkes, A.S., Horick, N.K., Healy, B.C., Shah, R., Bensaci, A.M., et al.; BACC Bay Tocilizumab Trial Investigators (2020). Efficacy of Tocilizumab in Patients Hospitalized with Covid-19. N. Engl. J. Med. *383*, 2333–2344.

Tang, L., Yin, Z., Hu, Y., and Mei, H. (2020). Controlling Cytokine Storm Is Vital in COVID-19. Front. Immunol. *11*, 570993.

Vourc'h, M., Roquilly, A., and Asehnoune, K. (2018). Trauma-Induced Damage-Associated Molecular Patterns-Mediated Remote Organ Injury and Immunosuppression in the Acutely Ill Patient. Front. Immunol. *9*, 1330.

Xiahou, Z., Wang, X., Shen, J., Zhu, X., Xu, F., Hu, R., Guo, D., Li, H., Tian, Y., Liu, Y., and Liang, H. (2017). NMI and IFP35 serve as proinflammatory DAMPs during cellular infection and injury. Nat. Commun. *8*, 950.

Yu, Y., Wang, X., Jin, T., Wang, H., Si, W., Yang, H., Wu, J., Yan, Y., Liu, G., Sang, X., et al. (2015). Newly Emergent Highly Pathogenic H5N9 Subtype Avian Influenza A Virus. J. Virol. *89*, 8806–8815.

Zhang, C. (2012). Hybridoma technology for the generation of monoclonal antibodies. Methods Mol. Biol. *901*, 117–135.

Zhang, Q., Raoof, M., Chen, Y., Sumi, Y., Sursal, T., Junger, W., Brohi, K., Itagaki, K., and Hauser, C.J. (2010). Circulating mitochondrial DAMPs cause inflammatory responses to injury. Nature *464*, 104–107.

Zhao, Y., Kuang, M., Li, J., Zhu, L., Jia, Z., Guo, X., Hu, Y., Kong, J., Yin, H., Wang, X., and You, F. (2021). SARS-CoV-2 spike protein interacts with and activates TLR41. Cell Res. *31*, 818–820.

Zhou, F., Yu, T., Du, R., Fan, G., Liu, Y., Liu, Z., Xiang, J., Wang, Y., Song, B., Gu, X., et al. (2020a). Clinical course and risk factors for mortality of adult inpatients with COVID-19 in Wuhan, China: a retrospective cohort study. Lancet *395*, 1054–1062.

Zhou, P., Yang, X.L., Wang, X.G., Hu, B., Zhang, L., Zhang, W., Si, H.R., Zhu, Y., Li, B., Huang, C.L., et al. (2020b). A pneumonia outbreak associated with a new coronavirus of probable bat origin. Nature *579*, 270–273.

Zhu, L., Yang, P., Zhao, Y., Zhuang, Z., Wang, Z., Song, R., Zhang, J., Liu, C., Gao, Q., Xu, Q., et al. (2020). Single-Cell Sequencing of Peripheral Mononuclear Cells Reveals Distinct Immune Response Landscapes of COVID-19 and Influenza Patients. Immunity *53*, 685–696.e3.

STAR★METHODS

KEY RESOURCES TABLE

REAGENT or RESOURCE	SOURCE	IDENTIFIER
Antibodies		
IFP35 neutralizing antibody	This paper	N/A
Bacterial and virus strains		
SARS-CoV-2 virus WIV04 strain	Zhou et al., 2020b	N/A
Influenza A virus A/Puerto Rico/8/1934 (H1N1)	Hoffmann et al., 2000	N/A
Biological samples		
Human Serum Specimens	Provided by Dr. Xiaoping Chen in Tongji hospital, Tongji Medical College, Huazhong University of Science and Technology	N/A
Mouse Serum Samples	This paper	N/A
Critical commercial assays		
Protein G Sepharose beads	GE Healthcare	17-0618-05
Human IFP35 ELISA kit	Aviva Systems Biology	OKEH02088
Human IL-6 ELISA kit	BioLegend	430501
Human TNF ELISA kit	BioLegend	430201
Mouse IFP35 ELISA kit	ELISA Genie	MOFI00328
Mouse TNF ELISA kit	BioLegend	430904
Mouse IL-6 ELISA kit	BioLegend	431304
Experimental models: Cell lines		
A549	ATCC	CRM-CRL-185
Vero E6	ATCC®	CRL-1586
MDCK (NBL-2)	ATCC	CCL-34
RAW264.7	ATCC	TIB-71
Experimental models: Organisms/strains		
Ifp35$^{-/-}$ mice	Xiahou et al., 2017	N/A
Wild type C57BL/6J mice	Guangdong Medical Laboratory Animal Centre	N/A
hACE2 transgenic mice	Jiang et al., 2020	N/A
SPF chicken embryonic eggs	Guangdong Wens Dahuanong Biotechnology Co., Ltd, Guangdong, China	N/A
BALB/c female mice	Guangdong Medical Laboratory Animal Centre	N/A
Oligonucleotides		
SARS-CoV-2 S gene amplified forward primer: 5′-CAATGGTTTAACAGGCAC AGG-3′	Jiang et al., 2020	N/A
SARS-CoV-2 S gene amplified reverse primer: 5′-CTCAAGTGTCT GTGGAT CACG-3′	Jiang et al., 2020	N/A
A/Puerto Rico/8/1934 (H1N1) genome RNA was reverse transcribed with primer AGCA AAAGCAGG	This paper	N/A

(*Continued on next page*)

Continued

REAGENT or RESOURCE	SOURCE	IDENTIFIER
PR8 viral NP gene amplified forward primer: 5′-ATCACTCACTGAGTGACATC-3′	This paper	N/A
PR8 viral NP gene amplified reverse primer: 5′-TCGTCCAATTCCACCAATCA-3′	This paper	N/A
Software and algorithms		
Prism 9.0	Graphpad	http://www.graphpad-prism.cn/
SPSS	IBM SPSS Statistics for Windows, version 26.0	https://www.ibm.com/analytics/spss-statistics-software
Other		
QuantStudio® 5 quantitative PCR	Applied Biosystems	SN: 27257220247
ELISA microplate reader	BioTek Instruments, INC	SN: 1803203

RESOURCE AVAILABILITY

Lead contact

Further information and requests for resources and reagents should be directed to and will be fulfilled by the lead contact Yingfang Liu (liuyingf5@mail.sysu.edu.cn).

Materials availability

There are restrictions to the availability of IFP35 neutralizing antibody due to the preparation of monoclonal antibody against IFP35 which has the neutralizing activity.

Data and code availability

All the data reported in this paper will be shared by the lead contact upon request. This paper does not report original code.

Any additional information required to reanalyze the data reported in this paper is available from the lead contact upon request.

EXPERIMENTAL MODEL AND SUBJECT DETAILS

Cell Lines

Cell lines of A549 (ATCC, CRM-CRL-185), Vero E6 (ATCC®, CRL-1586) and MDCK (NBL-2) (ATCC, CCL-34) were purchased from American Type Culture Collection (ATCC) and maintained in Dulbecco's modified Eagle's medium (DMEM, GIBCO, C11965500CP) supplemented with 10% fetal bovine serum (FBS, GIBCO, 10270106). RAW264.7 cells (ATCC, TIB-71) were purchased from ATCC and cultured in RPMI 1640 medium (GIBCO, C11875500BT).

Virus Strain

SARS-CoV-2 virus WIV04 strain was identified and isolated in Wuhan Institute of Virology, CAS. The virus was propagated in Vero E6 cells. The virus titer was determined using tissue culture infectious dose 50 ($TCID_{50}$) assay (Zhou et al., 2020b). Influenza A virus A/Puerto Rico/8/1934 (H1N1) (PR8) was rescued from 8 plasmids using reverse genetic method (Hoffmann et al., 2000), propagated in SPF chicken embryonic eggs (Guangdong Wens Dahuanong Biotechnology Co., Ltd, Guangdong, China), and purified by sucrose density gradient centrifugation. The virus titer was determined in MDCK cells by plaque assay (Yu et al., 2015).

Mice

All the *Ifp35*$^{-/-}$ mice are on the C57BL/6J background. 8-week-old sex-matched mice were used unless described otherwise. Wild-type mice (C57BL/6J) were purchased from Guangdong Medical Laboratory Animal Centre. Human angiotensin converting enzyme 2 (hACE2) transgenic mice were produced as previously described (Jiang et al., 2020). HFH4-hACE2 transgenic mice were maintained under specific pathogen free (SPF) conditions approved by the Institutional Animal Care and Use Committee of Wuhan Institute of Virology. *Ifp35*$^{-/-}$ homozygous knockout mice were produced as previously described (Xiahou et al., 2017). The mice were maintained under SPF conditions approved by the Institutional Animal Care and Use Committee of Sun Yat-Sen University.

Human Blood Samples

All the COVID-19 serum specimens were obtained from affiliated Tongji hospital, Tongji Medical College, Huazhong University of Science and Technology. Sera were separated and stored at −80°C. The informed consents were obtained from all participants and approved by the research ethics committee of Tongji Medical College, Huazhong University of Science and Technology

(TJ-C20201103). Uninfected volunteers were recruited from Tongji hospital, Tongji Medical College, Huazhong University of Science and Technology, and Guangdong Provincial Key Laboratory of Colorectal and Pelvic Floor Diseases, the Sixth Affiliated Hospital, School of Medicine, Sun Yat-sen University (IRB [2020] 004). All the serum was separated and stored at −80°C.

Diagnosis and classification of patients

The COVID-19 patients (Table S1) were from affiliated Tongji hospital, Tongji Medical College, Huazhong University of Science and Technology. The patients were diagnosed with SARS-CoV-2 infection on the basis of detecting viral nucleic acid in nasal swabs. The patient's condition was classified in accordance with *the sixth edition of the Diagnostic and Treatment Plan for Novel Coronavirus Pneumonia* issued by the National Health Commission of the People's Republic of China. Severely-ill patient was defined when any of the following was met: dyspnea, respiration rate (RR) $\geq$ 30 times/min; oxygen saturation by pulse oximeter $\leq$ 93% in resting state; partial pressure of arterial oxygen (PaO_2) to fraction of inspired oxgen (FiO_2) ratio $\leq$ 300 mm Hg (l mm Hg = 0.133 kPa). Severely-ill patient was defined when any of the following was met: respiratory failure and mechanical ventilation; shock; combine with multi-organs failure and admitted in intensive care unit (ICU).

Ethics Statement

All the animal experiments were conducted in accordance with the Regulations for the Administration of Affairs Concerning Experimental Animals approved by the State Council of the People's Republic of China. All the experiments referred to SARS-CoV-2 viruses were conducted in a biosafety level 3 laboratory, approved by the Institutional Animal Care and Use Committee of Wuhan Institute of Virology, Chinese Academy of Science, permission number WIVA05202007. The animal experiments of influenza virus were approved by Institutional Animal Care and Use Committee, Sun Yat-Sen University, permission number SYSU-IACUC-2019-B066.

METHOD DETAILS

Reagents

Enzyme linked immunosorbent assay (ELISA) kits of hIFP35 (OKEH02088) was purchased from Aviva Systems Biology (USA), while for mouse IFP35 (MOFI00328) from ELISA Genie (London, United Kingdom), for hIL-6 (430501) and hTNF(430201) from BioLegend (USA), and for mTNF (430904) and mIL-6 (431304) from BioLegend (USA).

Anti-IFP35 preparation and activity test

IFP35 neutralizing antibody was self prepared and purified in the lab according to the ordinary hybridoma method (Zhang, 2012). Briefly, C57BL/6J mice were immunized with human IFP35 protein. The spleen cells of the mice were collected and fused with myeloma cells. The positive hybridoma cells were selected. Homogeneous hybridoma cells were proliferated and injected into 8-12 week old BALB/c female mice to produce the ascites antibody. The neutralizing activity of the antibody against IFP35 was confirmed using LPS induced mouse sepsis mode.

The antibody in the crude ascites fluid was bound and purified from protein G Sepharose beads (17-0618-05, GE Healthcare) The neutralizing activity of the purified monoclonal antibody was determined in LPS-induced C57BL/6J septic mouse model (Grodzki and Berenstein, 2010).

ELISA

ELISA was conducted according to the manual instructions. Briefly, 100 μl of serially titrated standards were added, samples or blank were diluted into the wells of pre-coated microplate. Each item had 2 replicates. The plate was covered with the lid and incubated at 37°C for 2 hours. The liquid was discarded and 100 μl of diluted biotinylated detector antibody were added into each well. The plate was covered with lid and incubated at 37°C for 1 hour. The liquid was discarded and the plate was washed 3 times with 1 × wash buffer. 100 μl of diluted avidin-HRP conjugate was added into each well and incubated at 37°C for 1 h. The liquid was discarded and the plate was washed 5 times with 1 × wash buffer. 90 μl TMB substrate was added to each well and incubated for 15 - 30 min at 37°C. The plate was protected from light. 50μl of stop solution was added to each well and the OD450 absorbance was read with a microplate reader (Hornbeck, 2015).

Cell stimulation

A549 cells or RAW264.7 cells were separately seeded into 12-well plates 24 h prior to the viral infection. The cells were washed twice with PBS, then each cell type was inoculated with 5MOI PR8 virus. After 1 hour's incubation, the cells were washed twice and supplied with normal DMEM without FBS. Meanwhile, phosphate buffered saline (PBS) and 100 ng/ml LPS were used as negative and positive control, respectively. The supernatant of the cells was collected at 6, 12 and 24 hours post stimulation, then applied for ELISA analysis. The experiments were individually repeated for 3 times.

Viral genome RNA determination

The experiment of SARS-CoV-2 genome RNA quantification was performed as previously described (Jiang et al., 2020). Briefly, the lung tissues of hACE2 mice were homogenized in RNALater, viral genome RNA was isolated with QIAamp® 96 virus QIAcube® HT kit

(QIAGEN). The S gene of SARS-CoV-2 was amplified with specific primers F: 5′-CAATGGTTTAACAGGCACAGG-3′, R: 5′-CT CAAGTGTCT GTGGATCACG-3′. The lung tissues of C57BL/6J mice were homogenized in RNALater, and total RNA was extracted using TRIzol® LS Reagent (Life technologies, USA).

Influenza A virus A/Puerto Rico/8/1934 (H1N1) (PR8) genome RNA was reverse transcribed with primer AGCAAAAGCAGG using PrimeScript II 1st strand cDNA Synthesis Kit (Takara, 6210A). PR8 viral NP gene was amplified with specific primers F: 5′-ATCACT-CACTGAGTGACATC-3′, R: 5′-TCGTCCAATTCCACCAAT CA-3′. The cDNA products were used as template for qPCR amplification using SYBR Green Master Mix (Applied Biosystems, A25742). Ten microliter qPCR reaction system was consist of 5 μl 2 × one step SYBR green mix, 0.5 μl of each primer (10 μM), 2 μl cDNA template and 2 μl nuclease free water. Amplification was performed in the following procedure: 50°C for 2 minutes, 95°C for 2 minutes followed by 40 cycles consisting of 95°C for 15 s and 60°C for 1 minute, then the final 95°C for 15 s and 60°C for 1 minute. The reaction of quantitative PCR was performed on QuantStudio® 5 (Applied Biosystems, Thermo Fisher Scientific). The data were analyzed by standard method (Jiang et al., 2020).

Lung Tissues Histopathology

H&E staining experiments were performed according to previous report (Feldman and Wolfe, 2014). All the mouse lung tissues were fixed in 4% paraformaldehyde for 24 hours, embedded in paraffin and cut into 4 μm sections. Then all the sections were stained with hematoxylin solution for 3-5 minutes, rinsed with tap water. Then the sections were treated with hematoxylin differentiation solution, and rinsed with tap water. After that, the sections were treated with hematoxylin scott tap bluing, and rinsed with tap water. The sections were dehydrated in 85% ethanol for 5 minutes, followed by in 95% ethanol for 5 minutes. Finally, the sections were stained with eosin dye for 5 minutes. After a series of dehydration, all the sections were sealed with neutral gum. Each section was examined under the microscope, with the slides randomly read and examined for tissue damage, necrosis, and inflammatory cellular infiltration.

QUANTIFICATION AND STATISTICAL ANALYSIS

Statistical significance was assigned when P values were < 0.05 and the statistical method was indicated in the corresponding figure legends. The Normally distributed measurement data were determined with unpaired Student's t test. The Non-normal distributed measurement data were determined by nonparametric Mann-Whitney U-test or Wilcoxon signed-rank test. Correlations between clinical parameters were analyzed by spearman's rank correlation coefficient. The statistical significance of differences for survival rates was determined with Log rank test or Fisher's exact test as described in figure legends. For all tests, P value < 0.05 was considered significant (*). $p < 0.01$, very significant (**). $p < 0.001$, extremely significant (***).